JOURNAL OF THERMOPHYSICS AND HEAT TRANSFER
Vol. 13, No. 3, July–September 1999

Predictions for Cryogenic Homogeneous Two-Phase Flows in a Choked Laval Nozzle

Ibrahim Sinan Akmandor*
Middle East Technical University, 06531 Ankara, Turkey
and
Toshio Nagashima†
University of Tokyo, Tokyo 113, Japan

The vapor-liquid, two-phase, inviscid, compressible flow in a converging-diverging nozzle is computed by high accuracy total-variation-diminishing and Newton–Raphson schemes. A homogeneous speed of sound definition based on flow quality and void fraction is presented, along with some gas dynamic relations. Analytical two-phase mass-flow expressions are also derived, and solutions are compared with those obtained from the numerical schemes. The computational results of void-fraction and Mach-number relation obtained for the Laval nozzle compare favorably with both schemes. Equilibrium and nonequilibrium numerical results for cryogenic nitrogen flow are also presented. Numerical mass flux at both choked and unchoked throat conditions agrees with experimental data, but some discrepancy is observed in the pressure profiles at the diffusing portion of the nozzle.

Nomenclature

A = Jacobian matrix
A_b = interfacial area density
$\tilde{A}$ = locally averaged Roe's Jacobian
$A(\xi)$ = nozzle cross-sectional area
a = speed of sound
C = mixture specific heat constant
E = total specific energy
e = specific internal energy
$\boldsymbol{F}$ = vector tensor containing conserved fluxes
H = total enthalpy
h = enthalpy
K = new parameter used in speed of sound expression, $1 + R_G X/C$
$\dot{m}$ = mass-flow rate
N_G = bubble number density
P_t = total pressure
p = pressure
$\boldsymbol{Q}$ = column vector containing conserved variables
R_G = vapor gas constant
S = control volume surface
T = local mixture temperature
$\boldsymbol{T}$ = source vector carrying the nonequilibrium two-phase change model
T_s = saturation temperature of subcooled nitrogen
t = time
u = axial velocity component
X = flow quality
α = void fraction
Γ = two-phase source term
γ = gas-phase specific heat ratio
θ = bubble density primitive variable, N_G/ρ
λ = quality source coefficient
ξ = axial distance
ρ = mixture density
Ω = control volume

Subscripts

G = vapor phase
L = liquid phase
t = total quantity

Superscripts

$\boldsymbol{F}^*$ = numerical flux
L = fluid state at left side of the interface
R = fluid state at right side of the interface
T = transpose
α^* = void fraction at choked nozzle location

I. Introduction

THE understanding of subcooled fluid flow is of vital importance to space propulsion, where large quantities of cryogens are first stored and then supplied to the combustion chamber by high-performance turbomachinery components. In that context the rocket turbopump-inducer performance has been the focus for many years,[1] but the associated two-phase fluid dynamics is still not very well understood. Tests show that the void fraction α and the flow quality X are important factors in the inducer performance.[2] A thorough evaluation of equilibrium and nonequilibrium models as applied to choked flow is presented in a recent review paper[3]; however, very little research specifically addresses the cryogenic range of a choked nozzle.

Although two-fluid or separated flow models exist,[4] a simpler homogeneous mixture flow model is used in this paper to test fully the suitability and the applicability range of a newly derived speed-of-sound expression based exclusively on the flow quality, void-fraction, liquid-vapor mixture density and pressure. If the velocity ratio between the two phases is close to unity, the use of this homogeneous model is a good approximation. The Laval nozzle is solved with two different algorithms. The first scheme is a second-order-accurate Newton–Raphson linearization algorithm, which solves the quasi-one-dimensional steady two-phase Euler equations.[5] The second scheme is a third-order-accurate total variation diminishing (TVD) Euler scheme using the approximate Riemann solution of Roe (see Refs. 6 and 7). The numerical flow results are compared with experimental mass flux and pressure data of Simoneau and Hendricks.[8] A widespread use of upwind schemes for high-speed compressible gas flow with shock waves leads to their application in the simulation of two-phase

Presented as Paper 98-0889 at the AIAA 36th Aerospace Sciences Meeting, Reno, NV, 12–15 January 1998; received 22 April 1998; revision received 15 February 1999; accepted for publication 2 March 1999.

*Associate Professor, Department of Aeronautical Engineering. Member AIAA.
†Professor, Department of Aeronautics and Astronautics.

flows. Recently, for instance, an approximate linearized Riemann solver for a two-fluid model has been discussed.[9] But the study in such directions seems to be not fully developed yet. The present attempt of TVD coding for the simpler homogeneous model gives a straightforward demonstration of the scheme applicability.

II. Formulation and Discretization

A. Governing Equations for Newton–Raphson Scheme

The assumption is made that the flow through a convergent-divergent nozzle of high length-to-diameter ratio is steady, inviscid, and quasi-one-dimensional. The governing mass and energy equations are written in algebraic form, respectively:

$$\dot{m} = \rho u A = \text{const} \tag{1}$$

$$h_t = (1 + R_G X/C\alpha)CT + \tfrac{1}{2}u^2 = \text{const} \tag{2}$$

The local vapor-liquid mixture specific heat constant C is defined as $C = XC_G + (1 - X)C_L$, where C_G and C_L are the specific heat for pure vapor and liquid phases, respectively. The latter values are based on the saturation pressure of nitrogen and have been kept constant. The thermal equation of state, the caloric equation of state, the void fraction α, and the flow quality X are given respectively as

$$p = (X/\alpha)\rho R_G T \tag{3}$$

$$E = e + u^2/2 = XC_G T + (1 - X)C_L T + u^2/2 \tag{4}$$

$$\alpha = 1 - (1 - X)(\rho/\rho_L) \tag{5}$$

$$X = \alpha(\rho_G/\rho) \tag{6}$$

The liquid phase density ρ_L is kept constant. The differential equations that are solved through the Newton–Raphson algorithm are the quality and the axial momentum equations

$$\frac{\mathrm{d}}{\mathrm{d}\xi}[X\rho u A(\xi)] = \Gamma A(\xi) \tag{7}$$

$$\frac{\mathrm{d}}{\mathrm{d}\xi}[(p + \rho u^2)A(\xi)] = p\frac{\mathrm{d}A}{\mathrm{d}\xi} \tag{8}$$

The source term coefficient Γ in the quality equation represents the liquid-vapor nonequilibrium phase-change model of Dobran[10] for the discharge of high-pressure subcooled liquid through a pipe into ambient pressure:

$$\Gamma = \Gamma_e - \Gamma_c$$

$$\Gamma_e = \begin{cases} \lambda A_b \rho_L (1-\alpha)\alpha\sqrt{R_G T_s}[(T - T_s)/T_s]; & T \geq T_s \\ 0; & T < T_s \end{cases} \tag{9}$$

$$\Gamma_c = \begin{cases} \lambda A_b \rho_G (1-\alpha)\alpha\sqrt{R_G T_s}[(T_s - T)/T_s]; & T < T_s \\ 0; & T \geq T_s \end{cases}$$

λ is a parameter controlling the level of evaporation and condensation. For very slow rates of phase change, Dobran suggests a value much less than unity. A_b is the interfacial area density defined as

$$A_b = \begin{cases} \alpha^{\frac{2}{3}}(4\pi N_G/3)^{\frac{1}{3}}; & \alpha \leq 0.5 \\ (1-\alpha)^{\frac{2}{3}}(4\pi N_G/3)^{\frac{1}{3}}; & \alpha > 0.5 \end{cases} \tag{10}$$

First, all of the algebraic equations (1–6) are Newton-linearized. Namely, the incremental changes $\mathrm{d}u$, $\mathrm{d}p$, $\mathrm{d}T$, $\mathrm{d}\alpha$ are expressed as linear expressions of the flow quality changes $\mathrm{d}X$ and the density change $\mathrm{d}\rho$. Therefore, quality X and mixture density ρ become the main dependent variables of the scheme. Second, the set of differential equations (7) and (8) is also linearized. As a final step, the implicit Newton–Raphson method solves for the quality $\mathrm{d}X$ and density $\mathrm{d}\rho$ changes belonging to the whole domain by inverting a banded large sparse matrix at each iteration. Details of the upwinding and discretization procedure are detailed in an earlier work.[5]

B. Governing Equations for TVD Scheme

The quasi-one-dimensional time-dependent finite volume Euler equation is expressed in conservative form as follows:

$$\frac{\partial}{\partial t}[A(\xi)\boldsymbol{Q}] + \frac{\partial}{\partial \xi}(\boldsymbol{F}) = \boldsymbol{T} \tag{11}$$

where the column vector $\boldsymbol{Q}$ contains the conserved variables, the vector $\boldsymbol{F}$ contains the conserved fluxes, and $\boldsymbol{T}$ is the source vector carrying the nonequilibrium and quasi-one-dimensional approximations. That is,

$$\boldsymbol{Q} = [\rho, X\rho, N_G, \rho u, \rho E]^T \tag{12}$$

$$\boldsymbol{F} = A(\xi)\left[\rho u, X\rho u, N_G u, (p + \rho u^2), (p + \rho E)u\right]^T \tag{13}$$

$$\boldsymbol{T} = \left[0, \Gamma A(\xi), 0, p\frac{\mathrm{d}A(\xi)}{\mathrm{d}\xi}, 0\right]^T \tag{14}$$

C. Discretization of the TVD Scheme and Boundary Conditions

The space discretization of the TVD scheme is based on a characteristic decomposition of the flux difference. The expansion shocks are removed by use of the entropy fix of Harten and Hyman (Ref. 7). Roe's approximate Riemann formulation is used for the space discretization along with first-order time stepping, as follows:

$$A(\xi)\left(\boldsymbol{Q}_i^{n+1} - \boldsymbol{Q}_i^n\right) = -\frac{\Delta t}{\Delta x}\left(\boldsymbol{F}^*_{i+\frac{1}{2}} - \boldsymbol{F}^*_{i-\frac{1}{2}}\right) + \Delta t(\boldsymbol{T}^n)$$
$$\boldsymbol{F}^*_{i+\frac{1}{2}} = \tfrac{1}{2}(\boldsymbol{F}_{i+1} + \boldsymbol{F}_i) - |\tilde{A}|_{i+\frac{1}{2}}\left(\boldsymbol{Q}^n_{i+1} - \boldsymbol{Q}^n_i\right) \tag{15}$$

Where $\tilde{A}_{i+1/2}$ is the local averaged Jacobian, which has the same form of $A = \partial\boldsymbol{F}/\partial\boldsymbol{Q}$. Within $\tilde{A}_{i+1/2}$ the primitive variables $\rho, X, \theta = (N_G/\rho), u, H = E + p/\rho$ are replaced by their respective density-weighted average[11] values calculated from the left and the right sides of the interface:

$$\tilde{\rho} = \sqrt{\rho^R \rho^L} \tag{16}$$

$$\tilde{X} = \frac{X^R\sqrt{\rho^R} + X^L\sqrt{\rho^L}}{\sqrt{\rho^R} + \sqrt{\rho^L}} \tag{17}$$

$$\tilde{\theta} = \frac{\theta^R\sqrt{\rho^R} + \theta^L\sqrt{\rho^L}}{\sqrt{\rho^R} + \sqrt{\rho^L}} \tag{18}$$

$$\tilde{u} = \frac{u^R\sqrt{\rho^R} + u^L\sqrt{\rho^L}}{\sqrt{\rho^R} + \sqrt{\rho^L}} \tag{19}$$

$$\tilde{H} = \frac{H^R\sqrt{\rho^R} + H^L\sqrt{\rho^L}}{\sqrt{\rho^R} + \sqrt{\rho^L}} \tag{20}$$

$$A = A(\xi)\begin{bmatrix} 0 & 0 & 0 & 1 & 0 \\ -Xu & u & 0 & X & 0 \\ -\theta u & 0 & u & \theta & 0 \\ -u^2 - \dfrac{\partial p}{\partial \rho} & \dfrac{\partial p}{\partial X\rho} & 0 & \dfrac{\partial p}{\partial \rho u} + 2u & \dfrac{\partial p}{\partial \rho E} \\ -\dfrac{\partial p}{\partial \rho}u - Hu & \dfrac{\partial p}{\partial X\rho}u & 0 & \dfrac{\partial p}{\partial \rho u}u + H & \left(1 + \dfrac{\partial p}{\partial \rho E}\right)u \end{bmatrix} \tag{21}$$

The corresponding eigenvalues are

$$\lambda_1 = u + a, \qquad \lambda_{2,3,4} = u, \qquad \lambda_5 = u - a$$

where a is the two-phase speed of sound derived in the following paragraph, Eq. (23). Second-and third-order-accurate spatial approximations are obtained by correcting the flux $\boldsymbol{F}^*_{i+1/2}$ using the MUSCL approach.[7] Furthermore, to achieve a TVD formulation, the gradients of the variables are limited using the Van–Albada differential limiter.

At the nozzle inlet, total pressure, saturation pressure, total temperature, void fraction, and bubble density N_G are input. Exit pressure is also specified. Flow quality, vapor-liquid mixture density ρ, temperature, Mach number, and inlet velocity are determined accordingly. At the nozzle exit all conserved variables are extrapolated from newly updated values at the exit of the computational domain. For choked nozzles the exit pressure accommodates the location of the shock wave.

III. Two-Phase Flow Relations

A. Two-Phase Speed of Sound

For a bubbly fluid the speed of sound at frequencies well below the bubble resonant frequency can be considerably smaller than that of pure liquid. In the derivation of the one-dimensional, two-phase speed-of-sound equation, the flow quality X is assumed to be constant. Hence, the sound speed, which is the speed of longitudinal wave propagation in an inviscid and nonheat-conducting medium, can be calculated from the thermodynamic relations of the medium[12]:

$$a^2 = \frac{p}{\rho}\left[\frac{\mathrm{d}p}{p}\Big/\frac{\mathrm{d}\rho}{\rho}\right]\Bigg)_{s,X} = \frac{\partial p}{\partial \rho}\Bigg)_{T,X} + \frac{1}{\rho^2}\left(\frac{\partial p}{\partial T}\right)^2_{\rho,X}\frac{T}{C_v} \tag{22}$$

From the void-fraction definition, the thermal equation of state, and the first law of thermodynamics, the relative changes in pressure and density of Eq. (22) can be evaluated under the assumption of constant entropy and quality. A slightly different approach would be to evaluate the two pressure gradients of the second expression within Eq. (22) by using the state equation (3). Either of these substitutions yields the following compact but exact formula:

$$a^2 = K(p/\alpha\rho) \tag{23}$$

where $K = 1 + R_G X/C$ is a new two-phase homogeneous parameter that replaces the specific heat ratio γ. The speed-of-sound expression is integrated by separation of variables for fixed flow quality X, allowing the following isentropic total-to-static relations to be obtained:

$$\frac{T_t}{T} = \left(1 + \frac{K-1}{2}\frac{K/\alpha}{\alpha + K - 1}M^2\right), \qquad \frac{p_t}{p} = \left(\frac{T_t}{T}\right)^{K/(K-1)} \tag{24}$$

$$\rho_t = \left\{(1-X)\frac{1}{\rho_L} + \left[\frac{1}{\rho} - (1-X)\frac{1}{\rho_L}\right]\left(\frac{T_t}{T}\right)^{1/(K-1)}\right\}^{-1}$$

The applicability of these isentropic analytic relations within the broad range of two-phase flow is very limited. If any interfacial transfer occurs, they are no longer valid. The temperature and velocity used in the homogeneous model must be argued in the average sense where instantaneous interchanges between gas and liquid do not violate the supposition of an adiabatic change of their uniform mixture. The similarity of these exact two-phase gas dynamic relations with their single-phase counterparts is apparent. Indeed, as the flow quality X and the void fraction α approach unity, the single-phase gas dynamic relations are exactly recovered.

B. Void Fraction and Mach-Number Relations

The main purpose here is to provide an analytic expression that can be easily used to evaluate local void fraction without having to perform difficult calculations or measurements. During the numerical runs for cryogenic quasi-one-dimensional nozzle flow, we found that the variation of the parameter K is relatively small, and the void fraction closely follows the Mach-number profiles. It will be beneficial to estimate the local void fraction from the local total and static temperature measurements along with local Mach number. Therefore, a monotonic Mach-void fraction relation is derived. By integrating the speed-of-sound expression in Eq. (23), the following relation between pressure and density is obtained:

$$P_t/P = [(\rho_t/\rho)(\alpha/\alpha_t)]^K = (T_t/T)^{K/(K-1)} \tag{25}$$

Where α_t is the void fraction associated with the total quantities. By using the definition of void fraction, the $T - \rho$ relation of Eq. (25), and the total-to-static relations of Eq. (24), the analytical void-fraction Mach-number relation is derived:

$$\left[\frac{(1/\alpha^* - 1)^{K-1}}{(1/\alpha - 1)^{K-1}}\left(1 + \frac{K-1}{2}\frac{K/\alpha^*}{\alpha^* + K - 1}\right) - 1\right]$$

$$* \left[\frac{1}{[(K-1)/2][(K/\alpha)/(\alpha + K - 1)]}\right] = M^2 \tag{26}$$

The isentropic assumption will restrict the application range of this equation. Therefore, Eq. (26) will only be compared to homogeneous equilibrium numerical results that are upstream of the shock location. The only parameter in this expression is the void fraction α^* evaluated at the choked throat. Values of α^* can be directly read from the numerical results.

C. Two-Phase Flow Mass-Flow Parameters

Mass-flow parameters are often used in propulsion systems where $\dot{m}\sqrt{T_t}/A(\xi)P_t$ is treated as a variable that is exclusively dependent on Mach number and flow properties. In the absence of work and heat transfer, T_t is constant while changes in P_t are used to evaluate losses. Therefore, for given cross sections $A(\xi)$, T_t, and P_t, it is possible to evaluate the mass-flow rate $\dot{m}$ once the local Mach numbers M, α, and K are known. Two different mass-flow parameters are derived. The first expression, which is derived from total-to-static relations of Eq. (24), is the homogeneous two-phase mass-flow parameter:

$$\left[\frac{\dot{m}\sqrt{T_t}}{A(\xi)P_t}\right] = \sqrt{\frac{K}{R_G X}}M\left(1 + \frac{K-1}{2}\frac{K/\alpha}{\alpha + K - 1}M^2\right)^{-(K+1)/2(K-1)} \tag{27}$$

The second expression is based on a two-equation model where each of the vapor and liquid phases is represented by two parallel stream tubes, each passing through its respective area A_G or A_L:

$$\dot{m}_G = X\dot{m} = \rho_G u_G A_G \tag{28}$$

$$\dot{m}_L = (1-X)\dot{m} = \rho_L u_L A_L \tag{29}$$

The liquid phase is incompressible, so that

$$P_t/\rho_L = p/\rho_L + u_L^2/2 \tag{30}$$

The vapor phase is assumed to follow the single-phase gas dynamic relations from which A_G is deduced. The assumption is also made that the pressure of the liquid phase is the same as that of the gas phase. A_L is found by inserting u_L and p from Eqs. (30) and (24) into Eq. (29). Two-equation, two-phase mass-flow parameter $\dot{m}\sqrt{T_t}/A(\xi)P_t$ is then deduced from the parallel liquid-vapor streams model by taking $A(\xi) = A_G + A_L$, that is,

$$\left[\frac{\dot{m}\sqrt{T_t}}{A(\xi)P_t}\right]^{-1} = X\sqrt{\frac{R_G}{\gamma}}M^{-1}\left(1 + \frac{\gamma-1}{2}M^2\right)^{(\gamma+1)/2(\gamma-1)}$$

$$+ (1-X)\sqrt{\frac{P_t/T_t}{2\rho_L}}\left[1 - \left(1 + \frac{\gamma-1}{2}M^2\right)^{-\gamma/(\gamma-1)}\right]^{-\frac{1}{2}} \tag{31}$$

The two-equation model is more realistic because it allows for a velocity slip, and, furthermore, it does not assume temperature equilibrium between the two phases.

IV. Results and Discussion

A. Two-Phase Analytical Results

Figure 1 shows the speed-of-sound equation (23) along with the expressions of Nguyen and Mallock given in Refs. 13 and 14, respectively. $K = 1 + R_G X/C$ has been taken as 1.0154, corresponding to a flow quality of $X = 0.1$. Mallock's equation is an approximation to Eq. (23), where K is replaced by the specific heat ratio γ of pure gas phase. At 1 atm Eq. (23) yields slightly lower speed-of-sound values but still agrees well with the approximate analytical results reported by the aforementioned researchers. At 10.70 atm Eq. (23) agrees best with the other analytical speed-of-sound formulas. The wide void-fraction range for which the speed-of-sound equation seems to hold is also a favorable indication that the two numerical solvers, which are intrinsically based on this speed-of-sound formula, may also apply for a wide range of inlet void fraction.

Figure 2 illustrates the details of the Laval nozzle geometry: 150 nodes were used in the axial direction, with 35 nodes within the throat, and 45 nodes around the probable shock location in the divergent portion of the nozzle. The computational nodes were identical for the TVD and the Newton–Raphson solvers. The inlet area was 8.360 cm^2, the exit area was 3.896 cm^2, and a throat area was 0.09926 cm^2.

In Fig. 3, the analytical equation (26) and numerical void-fraction Mach-number relations are compared for three inlet void fractions: 0.1, 0.5, 0.8. Both numerical and analytical curves exhibit a monotonic pattern between void fraction and Mach number. The throat void number α^* can be read directly from the numerical solution plotted in the same figure, from the location where Mach number reaches unity. Hence, by using Eq. (26), a preliminary estimate of the void fraction can be achieved if the local Mach number and inlet void fraction are given.

Figure 4 shows the variation in homogeneous mass-flow parameter vs Mach number. The top curve corresponds to an inlet void fraction of 0.1, and the bottom curve to an inlet void fraction of 0.99. The choked Mach number is closer to unity for low inlet void fractions. For the higher inlet void fractions, the maximum mass-flow parameter occurs at a Mach number larger than unity. This discrepancy is caused by the parameter K, which is too low when compared to γ. In the limit of the highest void fraction, the peaked Mach number again shifts close to unity because the flow condition becomes almost only gas phase.

Figure 5 shows the analytical two-equation, two-phase mass-flow parameter vs Mach number. The highest mass-flow curve corresponds to the lowest inlet void fraction of 0.1. The low inlet void

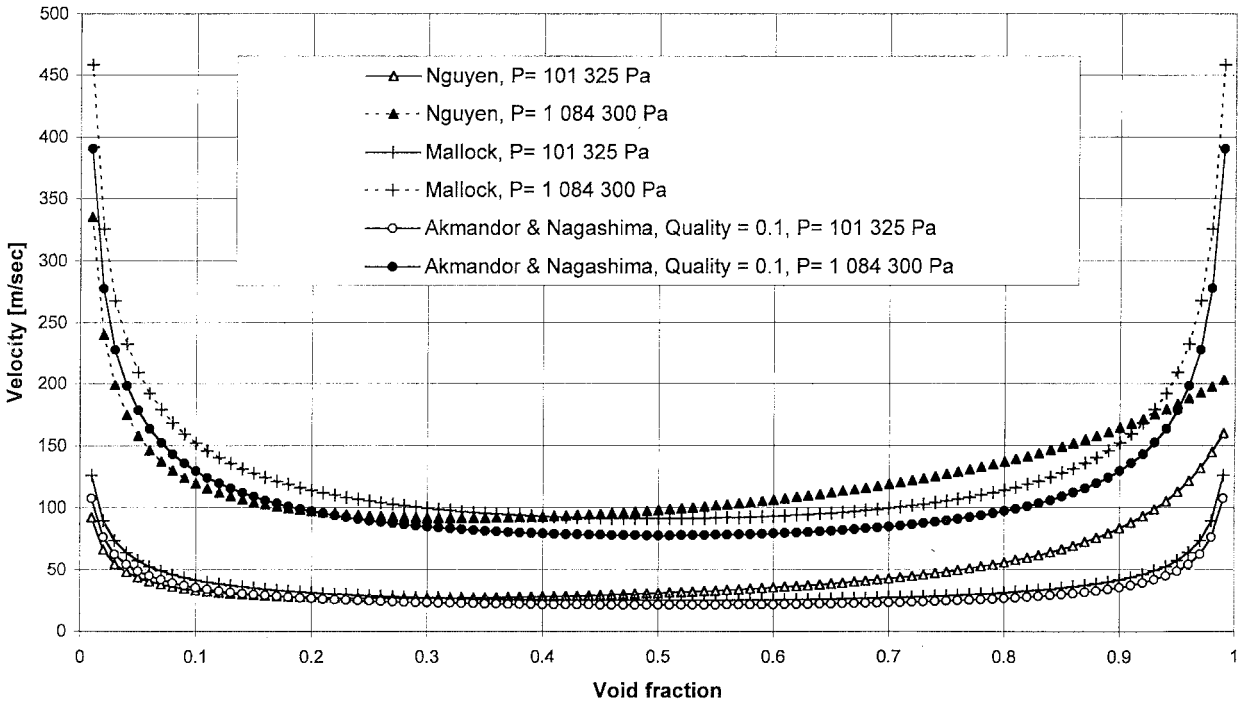

Fig. 1 Cryogenic two-phase speed of sound for homogeneous vapor-liquid nitrogen mixture.

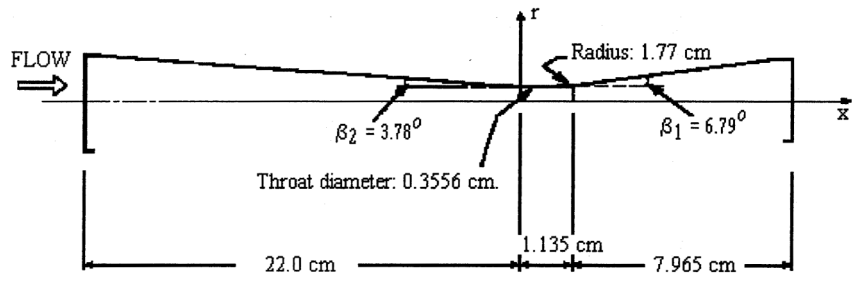

Fig. 2 Convergent-divergent nozzle geometry of Simoneau and Hendricks.[8]

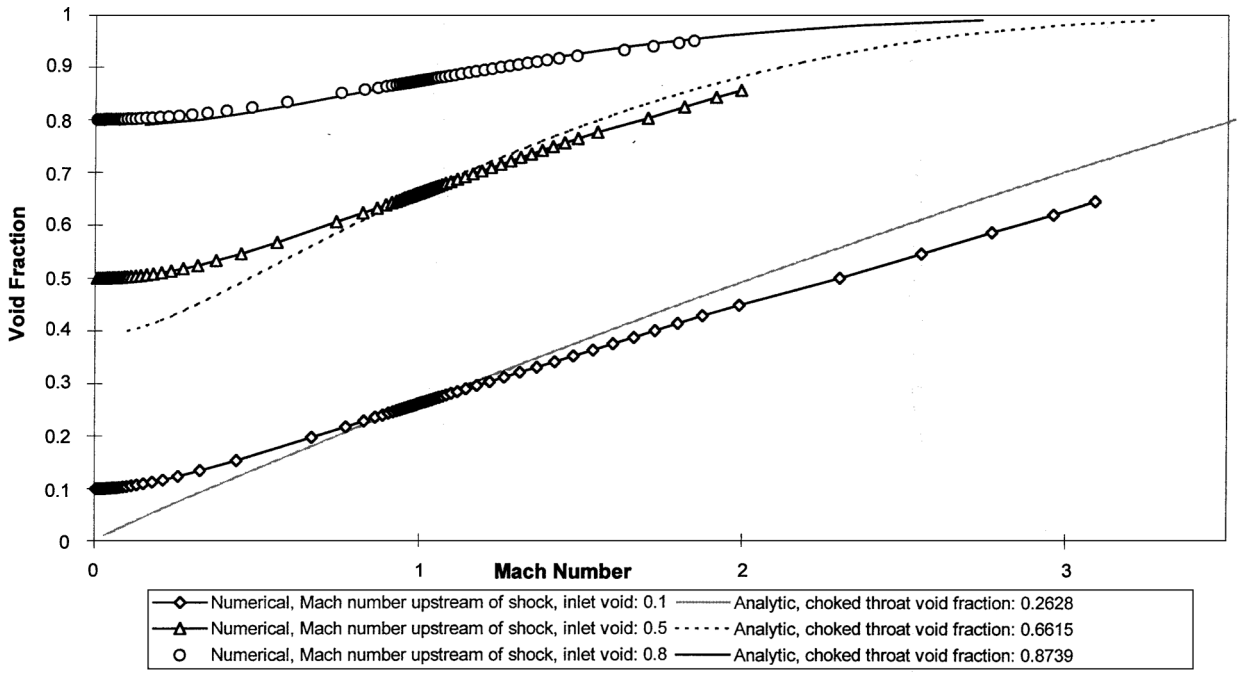

Fig. 3 Analytical and numerical void-fraction Mach-number relations: Pt = 2.26 MPa.

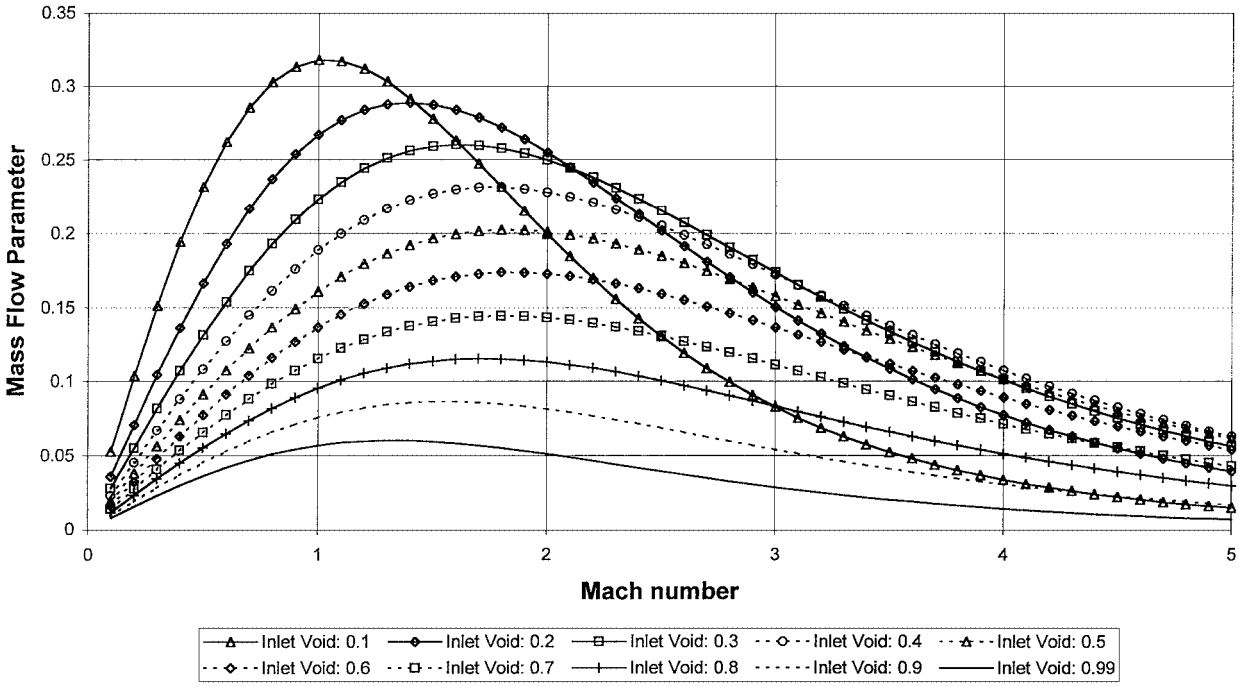

Fig. 4 Homogeneous two-phase mass-flow parameter: inlet Tt, 109.9 K; Pt, 2.26 MPa.

fraction causes high inlet density and consequently high mass-flow rates through the nozzle. As this flow contains more liquid phase, the Mach number at the choked throat shifts from unity to higher values. The lowest curve corresponds to an inlet void fraction of 0.99. As the mixture is mostly in vapor phase, the choked Mach number is unity.

B. Two-Phase Numerical Results

Figure 6 is an assessment of the grid dependency of the numerical solution. Eight different runs have been investigated. For both equilibrium and nonequilibrium runs increasing the grid node number from 150 to 200 does not affect the shock strength and shock location. As a further evaluation of the accuracy of the numerical solutions, the mass flux through each node has been computed, and their standard deviation from the throat mass flux rate is given in Table 1. The related experimental and numerical mass flux is also reported in Table 1. The difference stays always less than 0.28%.

The working fluid is subcooled liquid-vapor nitrogen. From the numerous data series reported by Simoneau and Hendricks,[8] the experimental series 133x and 135x have been chosen because they

Table 1 Inlet values and numerical mass flux accuracy

Experimental series number	Inlet T_t, K	Inlet P_t, MPa	Back P, MPa	Saturation P, MPa	Experimental mass flux, kg/m^2/s	Numerical mass flux, kg/m^2/s	Mass flux standard deviation within nodes
1331	109.1	4.71	3.60	1.39	43,700	43,700	0.00017
1332	109.4	4.65	1.77	1.42	56,500	56,410	0.00001
1333	109.9	4.63	0.54	1.46	61,600	61,430	0.00003
1351	109.9	2.26	1.62	1.46	33,400	33,420	0.00004
1353	110.9	2.25	1.22	1.51	33,300	33,240	0.00007

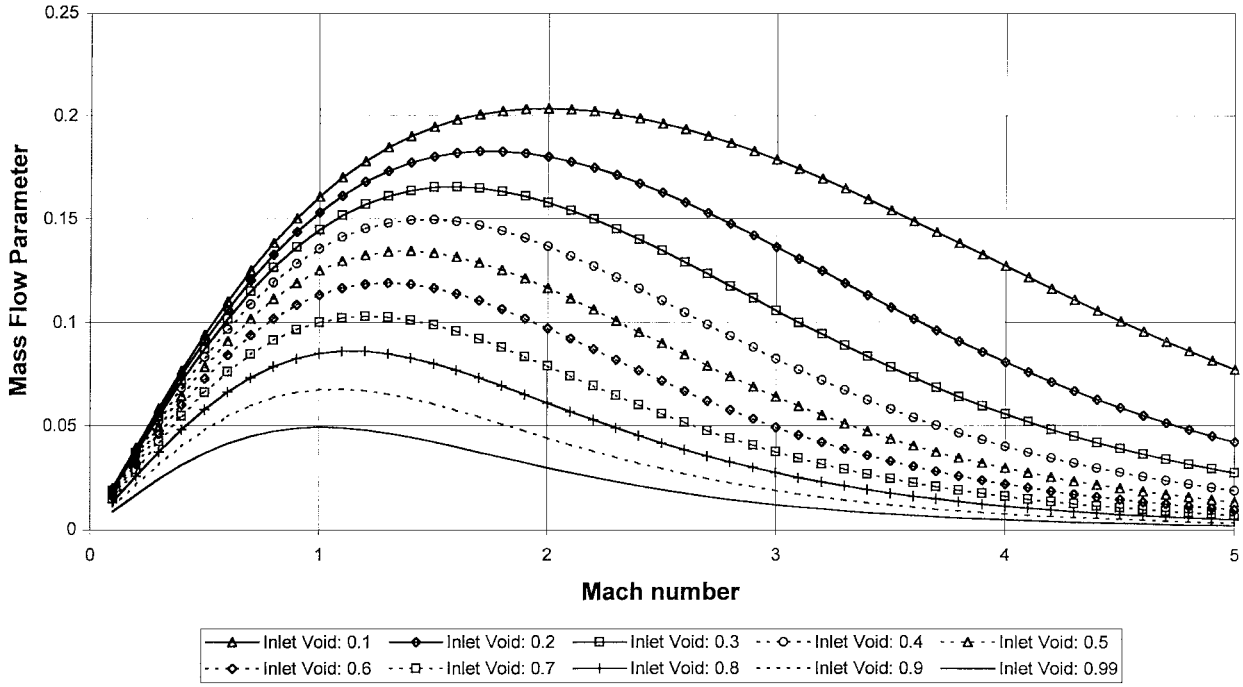

Fig. 5 Two-equation, two-phase mass-flow parameter: inlet Tt, 109.9 K; Pt, 2.26 MPa.

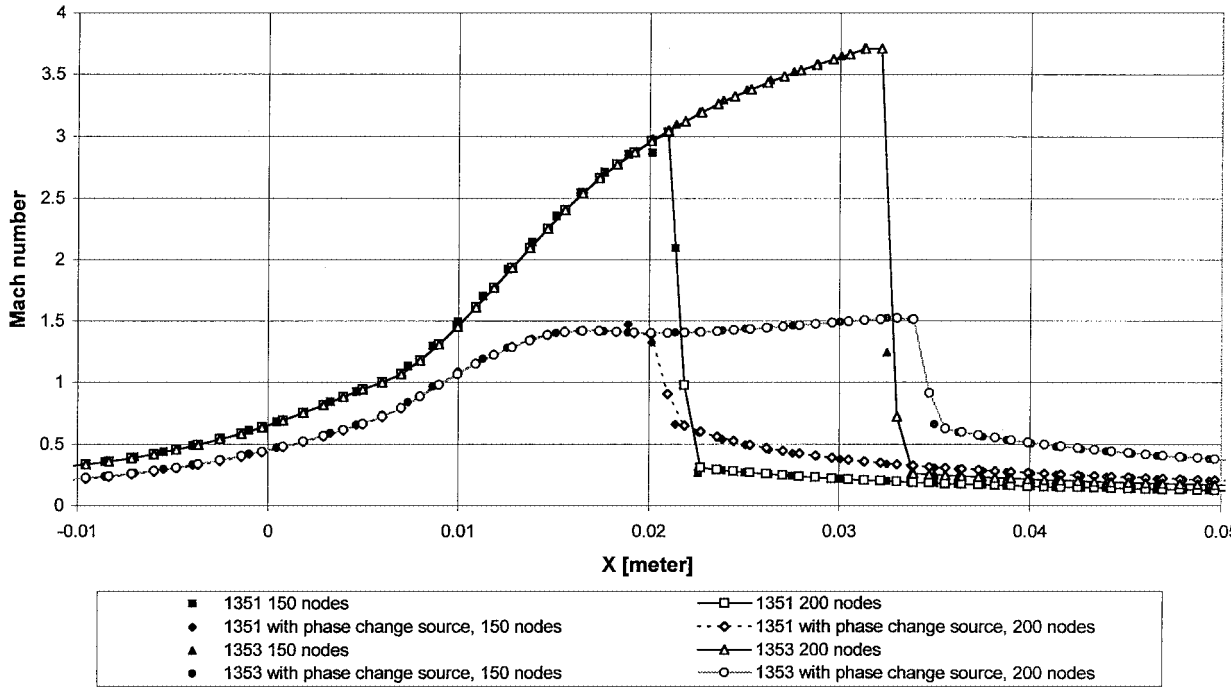

Fig. 6 Grid dependency of the numerical solutions.

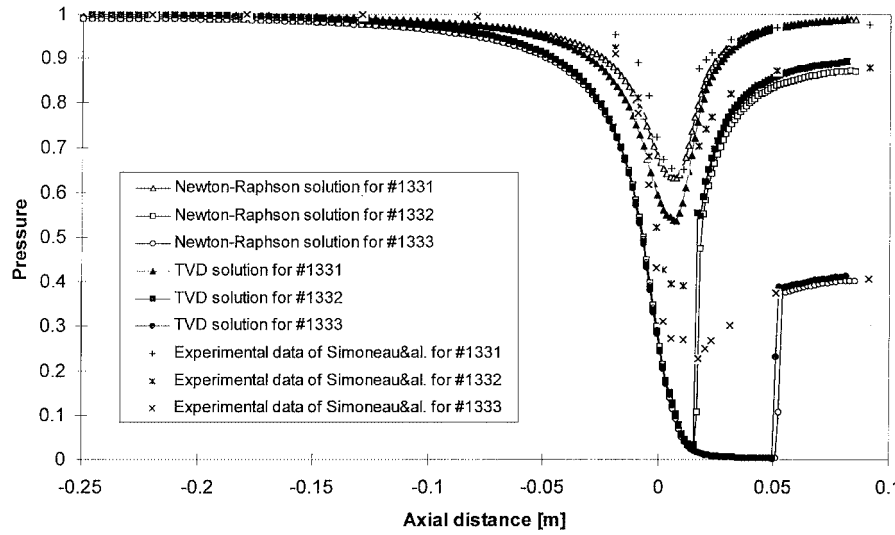

Fig. 7 Nitrogen axial numerical and experimental pressure profiles for inlet pressures around 4.65 MPa.

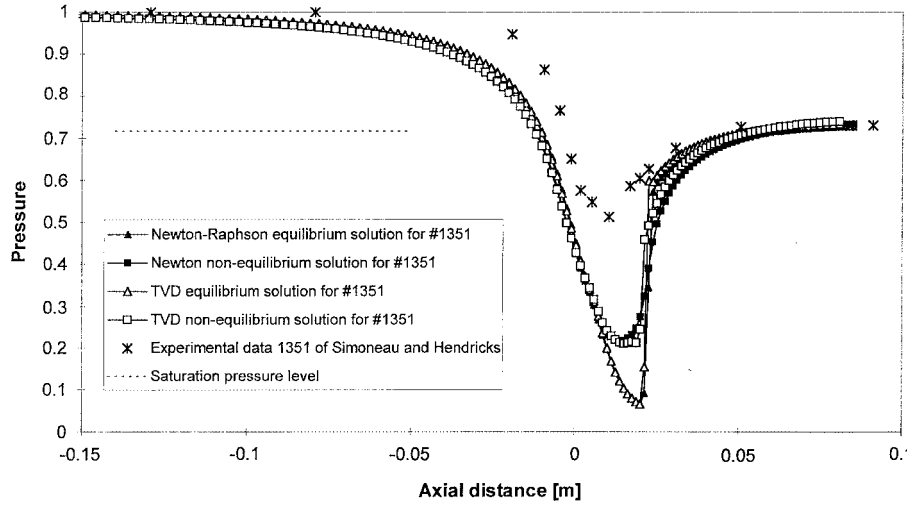

Fig. 8 Numerical equilibrium and nonequilibrium pressure profiles for inlet pressure: 2.26 MPa.

present axial pressure profiles over a wide range of both choked and unchoked backpressure data with the closest temperature tolerance. Also, the data series 135x is categorized as having an inlet stagnation pressure close to saturation pressure (Table 1). The numerical solutions are obtained from the TVD code and the Newton–Raphson code, and the corresponding results are plotted together. In all remaining results (Figs. 7–11) the TVD solutions agree very well with those of the Newton–Raphson scheme.

In Fig. 7 a set of numerical runs is presented and compared with the corresponding axial pressure data (#133x series) of Simoneau and Hendricks.[8] This set corresponds to an inlet pressure around 4.65 MPa. The backpressure is also input and is specified in Table 1 along with the corresponding saturation pressures. The results have been nondimensionalized with respect to the inlet total pressures given in Table 1. The experimental pressures are also plotted. Run #1331 is an all-subsonic flow, and the agreement with the numerical results is better than the other runs. Runs #1332 and 1333 are choked, and the flow is supersonic after the throat. The flow continues to accelerate in the divergent section up to the strong normal shock downstream of the nozzle. Figure 7 also shows that the shock location does move toward the exit plane as the backpressure is decreased from 3.60 to 1.77 MPa. In this portion of the nozzle, the experimental data again do not agree with the numerical results. This discrepancy must be further investigated.

Finally, Figs. 8–11 report equilibrium and nonequilibrium numerical results for an inlet pressure of 2.26 MPa. No related data are available for comparison. The quality equation now incorporates a nonequilibrium source term λ described earlier in Eq. (9). Solutions with $\lambda = 0$ (equilibrium) and 0.01 (nonequilibrium) are given in these figures.

Figure 8 illustrates the axial pressure profiles of such runs. Although the characteristics of both two-phase codes are very different, the agreement between them is good. The corresponding experimental data (#1351) are also plotted. The nonequilibrium results yield slight improvement in the agreement with the experimental plots, but their discrepancy is still significant and needs to be further studied probably on the physical ground.

The results in Figs. 9–11 illustrate the effect of the source term coefficient λ on the flowfield variables, specifically the Mach number M, the void fraction α, and the flow quality X. From Figs. 9 and 10 one-to-one correspondence between the Mach number and the void-fraction axial profiles can be seen. The supersonic portions of the nonequilibrium Mach-number profiles also reflect the effect of geometrical curvature near the throat. In contrast to the Mach-number profiles, the void-fraction axial profiles downstream of the shock are more influenced by nonequilibrium phase change. The equilibrium quality axial profiles shown in Fig. 11 are less influenced by the strong normal shock. In the nonequilibrium case the

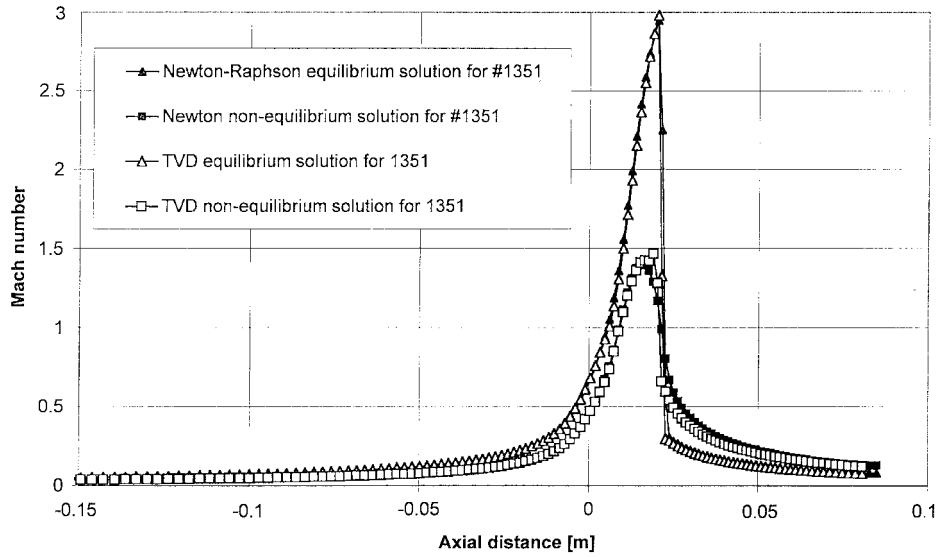

Fig. 9 Numerical equilibrium and nonequilibrium Mach-number profiles for inlet pressure: 2.26 MPa.

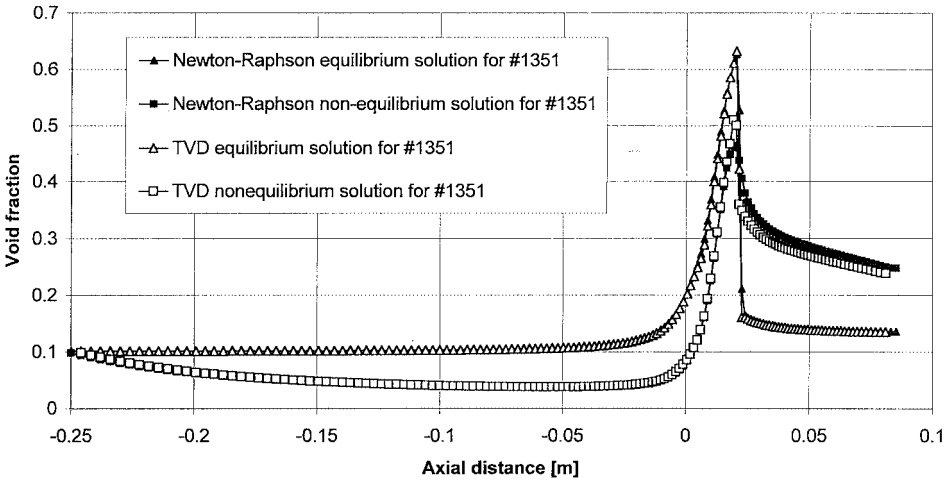

Fig. 10 Numerical equilibrium and nonequilibrium void fraction profiles for inlet pressure: 2.26 MPa.

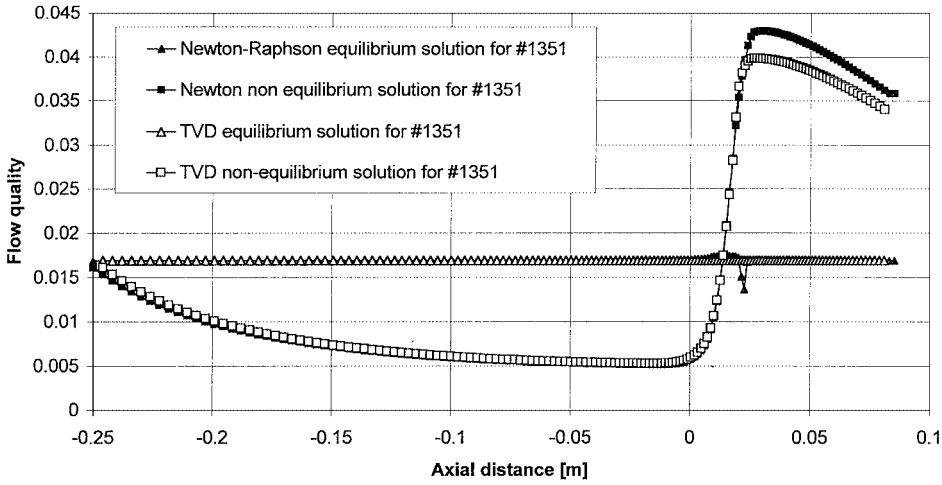

Fig. 11 Numerical equilibrium and nonequilibrium flow quality profiles for inlet pressure: 2.26 MPa.

flow quality decreases near the inlet at a rate corresponding to the subcooled temperature, becomes almost constant until the throat, and finally exhibits a sharp rise caused by shock-wave formation. Toward the exit, there is a small disagreement between the TVD and the Newton–Raphson results, which probably indicates the strongly coupled nature of the Newton–Raphson algorithm. In all cases at the nozzle exit, the nonequilibrium Mach number, flow quality, and void-fraction values are higher than respective equilibrium values, showing the strong interaction of flow expansion and phase change.

V. Conclusion

Two Euler algorithms were used for solving the homogeneous two-phase, compressible subcooled nozzle flow. New speed-of-sound, total-temperature, total-pressure, and total-density expressions have been defined. Satisfactory agreement has been obtained with empirical speed-of-sound results.

Except for pressure and mass flux, very few two-phase flow experimental data are available under cryogenic conditions. Therefore, there is a need for solvers capable of predicting cryogenic flow properties. The present numerical calculations, in spite of restrictions caused by simplified flow modelling, showed some agreement with the experimental mass flux through a nozzle with choked and unchoked conditions. Pressure field discrepancy at the rapidly diffusing portion needs to be further investigated on the physical ground. The shock strength and location are functions of backpressure and inlet void fraction.

References

[1]Jakobsen, J. K., and Keller, R. B., Jr., "Liquid Rocket Engine Turbopump Inducers," NASA SP-8052, May 1971.

[2]Yamada, H., Watanabe, M., Hasegawa, S., and Kamijo, K., "The Performance of a Cryogenic Pump for the Two-Phase Flow Condition," National Aerospace Lab., NAL TR-870, Kakuda Research Center, Sendai, Japan, March 1985 (in Japanese).

[3]Elias, E., and Lellouche, G. S., "Two-Phase Critical Flow," *International Journal of Multiphase Flow*, Vol. 20, Supplement, Aug. 1994, pp. 91–168.

[4]Delhaye, J. M., "Jump Conditions and Entropy Sources in Two Phase Systems. Local Instant Formulation," *International Journal of Multiphase Flow*, Vol. 1, No. 3, 1974, pp. 395–409.

[5]Akmandor, I. S., and Nagashima, T., "Newton–Raphson Solution of Cryogenic Homogeneous Two-Phase Flow in Convergent-Divergent Nozzles," *Transactions of the Japan Society for Aeronautical and Space Sciences*, Vol. 40, No. 127, 1997, pp. 40–58.

[6]Ishizaki, S., Akmandor, I. S., and Nagashima, T., "Numerical Analysis of Vapour-Liquid Two Phase Flow by Using a TVD Scheme," *Proceedings of the 34th Aeroengine and Space Propulsion Conference*, Aerospace Propulsion Div., Japan Society for Aeronautical and Space Sciences, Tokyo, 1994, pp. 230–235 (in Japanese).

[7]Hirsch, C., *Numerical Computation of Internal and External Flows*, Vol. 2, Computational Methods for Inviscid and Viscous Flows, Wiley, New York, 1988, pp. 61–70, 460–472.

[8]Simoneau, R. J., and Hendricks, R. C., "Two-Phase Choked Flow of Cryogenic Fluids in Converging-Diverging Nozzles," NASA TP 1484, July 1979.

[9]Toumi, I., and Kumbaro, A., "An Approximate Linearized Riemann Solver for a Two-Fluid Model," *Journal of Computational Physics*, Vol. 124, No. 2, 1996, pp. 286–300.

[10]Dobran, F., "Liquid and Gas Phase Distribution in a Jet with Phase Change," *Journal of Heat Transfer*, Vol. 110, No. 4A, 1988, pp. 955–960.

[11]Roe, P. L., "Approximate Riemann Solvers, Parameter Vectors and Difference Schemes," *Journal of Computational Physics*, Vol. 43, No. 2, 1981, pp. 357–372.

[12]Pai, S. I., *Two Phase Flows*, Vol. 3, Vieweg Tracts in Pure and Applied Physics, edited by K. Oswatitch, Vieweg, Braunschweig, Germany, 1977, pp. 56–80.

[13]Fischer, R., "Calculation of the Discharge Characteristic of an Orifice for Gas-Liquid Annular-Mist Flow," *International Journal of Multiphase Flow*, Vol. 21, No. 5, 1995, pp. 817–835.

[14]Nakoryakov, V. E., Pokusaev, B. G., and Shreiber, I. R., *Wave Propagation in Gas-Liquid Media*, 2nd ed., edited by A. E. Bergles, Begell House CRC Press, Boca Raton, FL, 1993, pp. 1–4.